

Planar InAlAs/InGaAs avalanche photodiode with 360 GHz gain×bandwidth product

Shuai Wang(王帅), Han Ye(叶焓), Li-Yan Geng(耿立妍), Fan Xiao(肖帆), Yi-Miao Chu(褚艺渺), Yu Zheng(郑煜), Qin Han(韩勤)

Citation: Chin. Phys. B, 2023, 32 (**9**): 098507. DOI: 10.1088/1674-1056/ace61b
Journal homepage: http://cpb.iphy.ac.cn; http://iopscience.iop.org/cpb

What follows is a list of articles you may be interested in

Analysis of high-temperature performance of 4H-SiC avalanche photodiodes in both linear and Geiger modes

Xing-Ye Zhou(周幸叶), Yuan-Jie Lv(吕元杰), Hong-Yu Guo(郭红雨), Guo-Dong Gu(顾国栋), Yuan-Gang Wang(王元刚), Shi-Xiong Liang(梁士雄), Ai-Min Bu(卜爱民), and Zhi-Hong Feng(冯志红)
Chin. Phys. B, 2023, 32 (**3**): 038502. DOI: 10.1088/1674-1056/ac9820

Theoretical analysis for AlGaN avalanche photodiodes with mesa and field plate structure

Ke-Xiu Dong(董可秀), Dun-Jun Chen(陈敦军), Qing Cai(蔡青), Yan-Li liu(刘燕丽), Yu-Jie Wang(王玉杰)
Chin. Phys. B, 2020, 29 (**8**): 088502. DOI: 10.1088/1674-1056/ab90f1

Performance improvement of 4H-SiC PIN ultraviolet avalanche photodiodes with different intrinsic layer thicknesses

Xiaolong Cai(蔡小龙), Dong Zhou(周东), Liang Cheng(程亮), Fangfang Ren(任芳芳), Hong Zhong(钟宏), Rong Zhang(张荣), Youdou Zheng(郑有炓), Hai Lu(陆海)
Chin. Phys. B, 2019, 28 (**9**): 098503. DOI: 10.1088/1674-1056/ab343f

An improved design for AlGaN solar-blind avalanche photodiodes with enhanced avalanche ionization

Yin Tang(汤寅), Qing Cai(蔡青), Lian-Hong Yang(杨莲红), Ke-Xiu Dong(董可秀), Dun-Jun Chen(陈敦军), Hai Lu(陆海), Rong Zhang(张荣), You-Dou Zheng(郑有炓)
Chin. Phys. B, 2017, 26 (**3**): 038503. DOI: 10.1088/1674-1056/26/3/038503

Bias-dependent timing jitter of 1-GHz sinusoidally gated InGaAs/InP avalanche photodiode

Ge Zhu(朱阁), Fu Zheng(郑福), Chao Wang(王超), Zhibin Sun(孙志斌), Guangjie Zhai(翟光杰), Qing Zhao(赵清)
Chin. Phys. B, 2016, 25 (**11**): 118505. DOI: 10.1088/1674-1056/25/11/118505

RAPID COMMUNICATION

Planar InAlAs/InGaAs avalanche photodiode with 360 GHz gain×bandwidth product

Shuai Wang(王帅)[1,2], Han Ye(叶焓)[1,2], Li-Yan Geng(耿立妍)[1,2], Fan Xiao(肖帆)[1,2], Yi-Miao Chu(褚艺渺)[1,2], Yu Zheng(郑煜)[1,2], and Qin Han(韩勤)[1,2,†]

[1] *Key Laboratory of Integrated Optoelectronics, Institute of Semiconductors, Chinese Academy of Sciences, Beijing* 100083, *China*
[2] *School of Electronic, Electrical and Communication Engineering, University of Chinese Academy of Sciences, Beijing* 100049, *China*

(Received 28 April 2023; revised manuscript received 6 July 2023; accepted manuscript online 11 July 2023)

This paper describes a guardring-free planar InAlAs/InGaAs avalanche photodiode (APD) by computational simulations and experimental results. The APD adopts the structure of separate absorption, charge, and multiplication (SACM) with top-illuminated. Computational simulations demonstrate how edge breakdown effect is suppressed in the guardring-free structure. The fabricated APD experiment results show that it can obtain a very low dark current while achieving a high gain×bandwidth (GB) product. The dark current is 3 nA at $0.9V_{\rm br}$, and the unit responsivity is 0.4 A/W. The maximum 3 dB bandwidth of 24 GHz and a GB product of 360 GHz are achieved for the fabricated APD operating at 1.55 μm.

Keywords: avalanche photodiode, planar, gain×bandwidth product, dark current

PACS: 85.60.Gz, 73.40.Kp, 81.15.Hi **DOI:** 10.1088/1674-1056/ace61b

1. Introduction

Avalanche photodiodes (APDs) are key components in the receiver of optical fiber communication system because they have internal gain to improve the sensitivity and dynamic range.[1–4] They can provide at least 10 dB higher signal to noise ratio than PIN photodiodes. InP was initially used as the avalanche material, since the APD epitaxial structure operating in the 1.3–1.6 μm band was grown on an InP substrate.[4,5] However, $In_{0.52}Al_{0.48}As$ (InAlAs), which is also lattice-matched with InP, is more suitable as the avalanche materials than InP, because the carrier ionization rate ratio k is lower than that of InP. InAlAs-APDs can obtain higher gain×bandwidth (GB) product and lower excess noise factor. The bandgap width of InAlAs is also higher than that of InP, which is beneficial to reduce the tunneling dark current of the APD,[6–8] and the temperature stability of the InAlAs-APDs has been strengthened due to the lower temperature dependence of the multiplication process.[9,10] The vertical illuminated structure APD can achieve optical coupling relatively easily, and it is not affected by the polarization during the absorption of optical signals.[11,12] Therefore, various vertical illumination InAlAs high-speed APDs have been extensively reported recently. However, most of the reported results are based on the multi-mesa structure, and the dark current of this structure is relatively large.[4,5,8,9,13–15]

In this paper, we propose a guardring-free planar InAlAs-APD with vertical top-illuminated SACM structure that can be fabricated by the selective Zn-diffusion process similar to the fabrication of conventional InP-APD.[16–18] The dark current is 3 nA at $0.9V_{\rm br}$, and the unit responsivity is 0.4 A/W. The maximum 3 dB bandwidth of 24 GHz and a GB product of 360 GHz are simultaneously achieved for the fabricated InAlAs-APD. These characteristics demonstrate the potential of the planar InAlAs-APD for optical communication system. Compared with mesa-type APD reports, their dark currents are relatively large due to the surface effect at the mesa sidewalls and with that a higher noise.[3,7,19,20] The dark current of Nada M, etc. has reached 100 nA, which will lead to relatively large noise in the actual use of the device.[20] Compared with other planar APD reports, the results of this device show significant improvement of GB while keeping a low dark current.[4,21,22]

2. Design of device structure and fabrication

APD was designed in the lattice-matched InGaAs/InAlAs/InP epitaxial material system. The epitaxial structure and the cross-section of the APD are shown in Table 1 and Fig. 1, respectively. It is grown by metal organic chemical vapor deposition (MOCVD) on a semi-insulating (SI) InP substrate. From the top P-contact diode and incident light window, follows a 1 μm InP cap layer. An InGaAsP grading layer is inserted to reduce hole pile-up between a low bandgap $In_{0.53}Ga_{0.47}As$ (InGaAs) absorption layer and a wide bandgap InP cap layer. The thickness of the InGaAs absorption layer is 600 nm. The InAlAs avalanche layer thickness of 100 nm is determined to maximize the GB product, while the dark current can also be maintained at a relatively low level simultaneously. The design of the charge layer is the

†Corresponding author. E-mail: hanqin@semi.ac.cn

© 2023 Chinese Physical Society and IOP Publishing Ltd

key to adjusting the internal electric field of the APD.[5] Here, the thickness is set to 50 nm, and the doping concentration is 9×10^{17} cm^{-3}. The p^+ active region is achieved by Zn selective thermal diffusion in the undoped InP cap layer. A Ti/Pt/Au P-contact is achieved by a photolithographic lift-off process. An AuGeNi/Au N-contact is evaporated on the same side of the substrate. A silicon nitride (SiN_x) passivation layer covers the whole APD surface.

Table 1. The epitaxial structure of SACM InGaAs/InAlAs/InP APD.

Layer	Material	Type	Doping (cm^{-3})	Thickness (nm)
Cap	InP	nid	undoped	1000
Grading	$Ga_{0.149}In_{0.851}As_{0.327}P_{0.673}$	nid	undoped	10
	$Ga_{0.286}In_{0.714}As_{0.619}P_{0.381}$	nid	undoped	10
	$Ga_{0.412}In_{0.588}As_{0.886}P_{0.114}$	nid	undoped	10
Absorption	$In_{0.53}Ga_{0.47}As$	nid	undoped	600
Transition	$In_{0.53}Ga_{0.35}Al_{0.12}As$	nid	undoped	33
	$In_{0.53}Ga_{0.23}Al_{0.24}As$	nid	undoped	33
	$In_{0.52}Ga_{0.12}Al_{0.36}As$	nid	undoped	33
Charge	$In_{0.52}Al_{0.48}As$	p^+	9×10^{17}	50
Avalanche	$In_{0.52}Al_{0.48}As$	nid	undoped	100
Buffer	$In_{0.52}Al_{0.48}As$	n^+	5×10^{17}	200
Contact	InP	n^+	5×10^{18}	600
Substrate	InP	S.I	S.I	

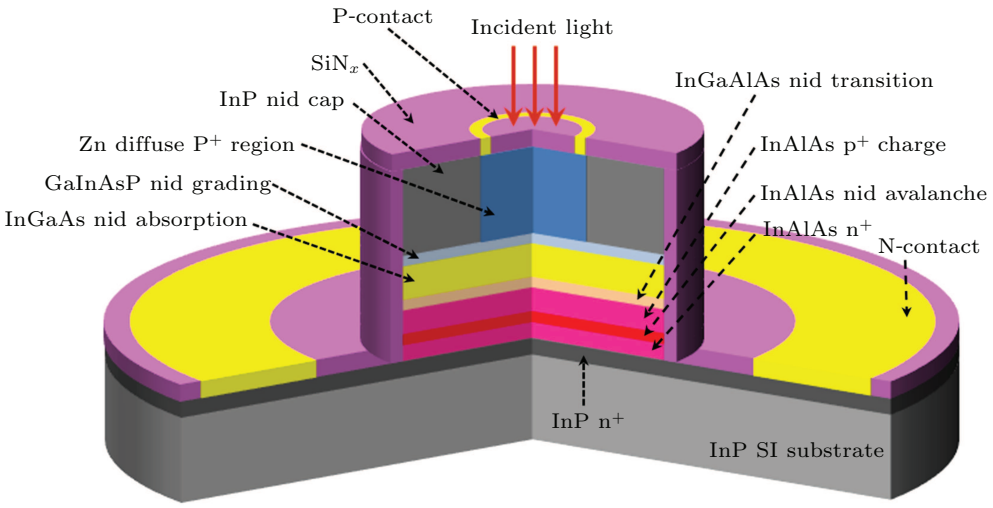


Fig. 1. Schematic 3D and cross-section of the top-illuminated APD.

Selective diffusion or ion implantation is required to confine the active area of the planar SACM APD. A spherical or cylindrical boundary will be formed at the edge by diffusion or ion implantation in planar APD as is shown in Fig. 1 and its curvature is greater than that of the central boundary. A higher local electric field will be formed at the diffusion edge boundary due to the curvature effect. For the traditional InP SACM APD, its p–n junction is realized by Zn diffusion, and the boundary of diffusion is the p–n junction of APD. When the APD is operating, the electric field in the p–n junction is the largest to generate avalanche gain. The electric field at the edge boundary is greater than that at the center boundary due to the curvature effect, so it will cause the p–n junction to breakdown earlier at the edge boundary than at the center boundary.[16–18] Serious APD edge breakdown leakage will even make the APD unable to work. Therefore, a guard ring is necessary at periphery of the APD to reduce the edge premature breakdown effect in traditional InP SACM APDs.[23] For the planar InAlAs SACM APD, the true p–n junction is located in the InAlAs avalanche layer, and the p–n junction is formed by epitaxy on a large plane. The electric field is the largest in the InAlAs avalanche layer in order to generate avalanche gain.[4,22] Figure 2(a) shows the two-dimensional electric field distribution of the guardring-free InAlAs planar structure using drift-diffusion model by computational simulation. The electric field intensity distributions are extracted along the grading and avalanche layer in the horizontal of the structure as shown in Fig. 2(b). It is found that the electric field in InAlAs p–n junction under the diffused active region is the largest when the device is biased, and it is lowered toward the periphery of the junction owing to the distance from the diffusion. The boundary of the Zn diffusion is in the grading layer.

Although the electric field at the diffusion edge boundary in the grading layer will be greater than that at the diffusion center boundary due to the curvature effect, the electric field here is much lower than that at the InAlAs avalanche layer, which is the true p–n junction. We confirmed that the strongest electric field is not applied at the Zn diffusion edge where edge breakdown is inclined to occur, because the p–n junction is formed at the hetero-interface between the InAlAs avalanche layer. So no special guard-ring design is needed to suppress the edge breakdown effect.

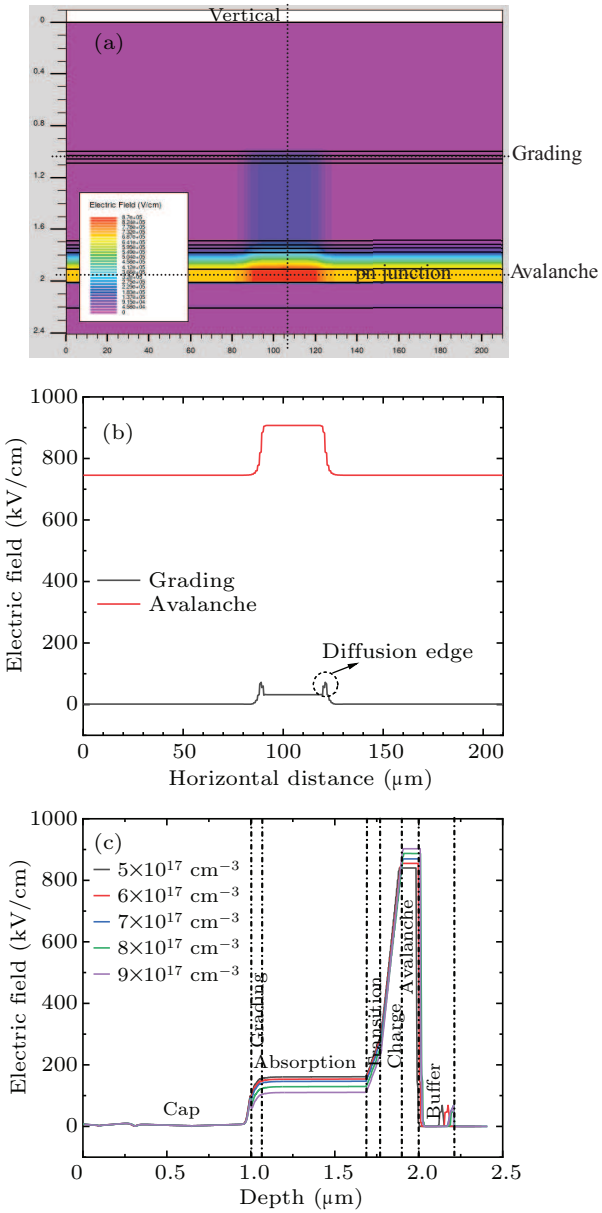


Fig. 2. The simulated two-dimensional electric field distribution (a) in horizontal along the grading and avalanche layer (b) and in vertical with different densities (c).

The results of adjusting the internal electric field distribution of the device vertical direction by charge layer with different densities are shown in Fig. 2(c). It can be seen from the figure that the electric field decreases in the absorption region and increases in the multiplication region with increasing the charge density. High electric field ($>$ 900 kV/cm) is achieved in the 100 nm avalanche region which is needed for the impact ionization, while the electric field remains quite low ($<$ 200 kV/cm) in the absorption region to avoid the tunneling dark current, when the doping concentration of the charge layer is 9×10^{17} cm^{-3}.

It is critical to calculate the band energy profiles resulting from device design, in order to predict device performance and thus be able to adjust the layer thickness and doping profiles of APD structures. Band energy distribution calculations have been performed for various applied bias voltages using 1D Poisson, drift-diffusion. Figure 3 depicts the calculated band energy curves without bias voltage (a) and at the 90% breakdown voltage (b). In the absence or with a small bias voltage, the electrons generated in the absorber will not be able to overcome the barrier of the charge layer to reach the n-contact. However, with the increase of the bias voltage, the potential barrier will be reduced, and the photogenerated electrons can flow into the avalanche layer to generate gain, which can be collected by the external circuit.

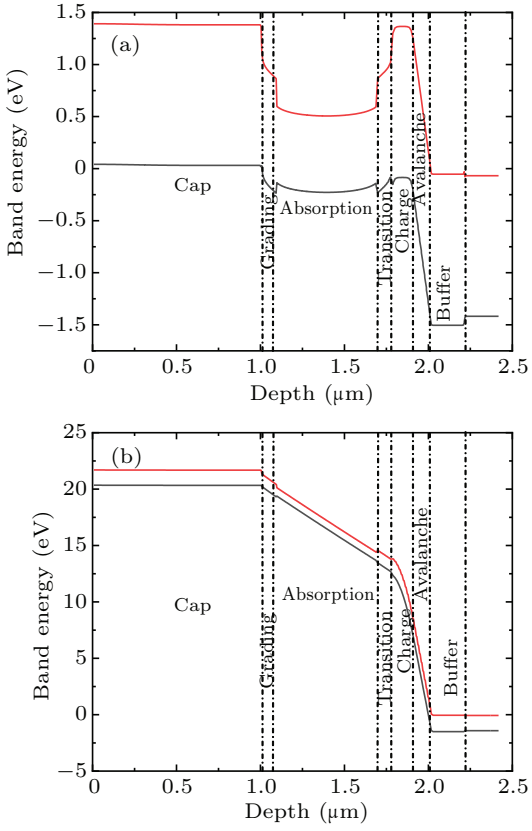


Fig. 3. Calculated band energy profile of the APD without bias voltage (a) and at 90% V_{br} (b).

3. Characteristics and discussion

Figure 4 is the dark current, photocurrent and operation gain versus reverse bias of a 15 μm diameter device at room temperature. The photocurrent and gain curves are under different incident light powers at the wavelength of 1.55 μm. The breakdown voltage (V_{br}) is defined as the bias voltage at which

the dark current is 100 μA.[24] The V_{br} is 26 V while the corresponding dark current is around 3 nA at $0.9V_{br}$. The low dark current is mainly due to the planar structure and the precisely designed charge layer to adjust the electric field. The punch-through voltage (V_{pt}) is 8 V, and the photoresponsivity at this bias can be defined as unity gain. The responsivity at unity gain is 0.4 A/W with different incident light power and the corresponding external quantum efficiency (η) is 32%. The measured responsivity is consistent with the calculated results of the 600 nm InGaAs epitaxial absorption layer.

It can be seen that all measured operational gains degrade significantly when the applied bias voltage exceeds V_{br}. This is due to the sharp increase in dark current, which accounts for the majority of the total current measured. Furthermore, it can be clearly seen that the maximum operating gain gradually decreases with increasing incident light power. This phenomenon is mainly caused by the space charge screening (SCS) effect. Photogenerated carriers will increase with the increase of incident light power. The photogenerated electrons are injected into the multiplication layer under high electric field to induce impact ionization. A large number of holes ionized in the multiplication layer accumulate at the heterojunction due to the slow drift speed, which reduces the net electric field and multiplication gain in the multiplication layer.

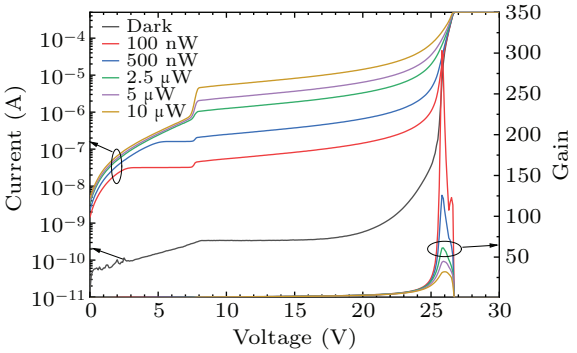


Fig. 4. The dark current, photocurrent and operation gain versus reverse bias of a 15 μm diameter device at room temperature.

Figure 5 shows the 3 dB optical to electrical (OE) response frequency characteristics of the fabricated APD device. It can be seen from Fig. 5(a) that the 3 dB bandwidth of the device is 1 GHz near V_{pt}, and sharply increases with the increase of the bias. As shown in Fig. 5(b), when the bias voltage is increased to 11 V, the 3 dB bandwidth of the device reaches the maximum value of 24 GHz. In addition, the bandwidth begins to slowly decrease as the voltage continues to increase, which is mainly determined by the GB product limitation. As shown in Fig. 5(c), the APD device can sustain the 3 dB bandwidth of approximately 12 GHz near the V_{br}.

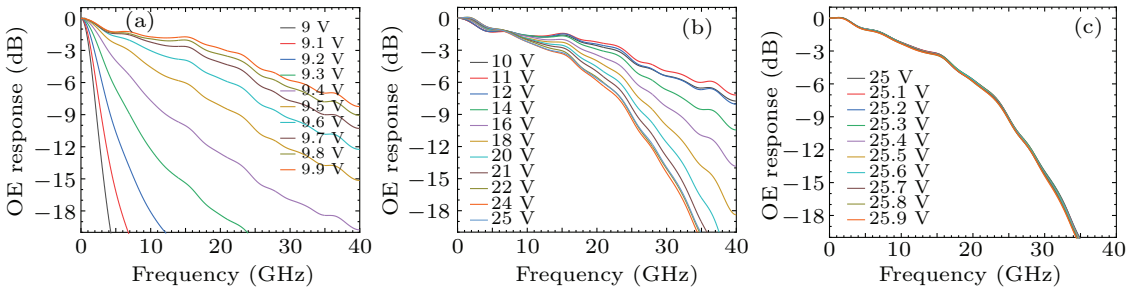


Fig. 5. The 3 dB OE response frequency characteristics of the APD.

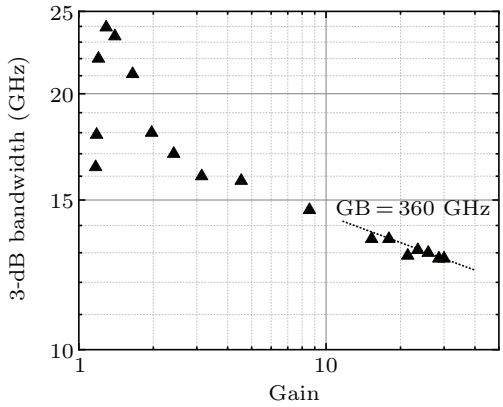


Fig. 6. The high-frequency response versus multiplication factor.

The high-frequency response versus multiplication gain is shown in Fig. 6. The multiplication factor gain in the figure is the result when the incident light power is 10 μW. The 3 dB bandwidth is low at unity gain and increases dramatically with gain. This is because the electric field in the absorption region is weak when the device is just punched through, and the photogenerated carriers do not reach their saturation drift velocity. As the voltage increases, the electric field in the absorption region gradually increases, the carrier drift velocity reaches saturation, and the 3 dB bandwidth reaches the maximum value of 24 GHz. The measured capacitance is 0.17 pF and the parasitic resistance is 50 Ω, so the maximum bandwidth is limited by both the RC time constant and the carrier transit time of the depletion layer. The 3 dB bandwidth of the device can be sustained at 12 GHz for a multiplication gain between 6 and 30, and then the GB product reaches 360 GHz.

4. Conclusion

In summary, a guardring-free planar structure InGaAs/InAlAs SACM-APD with top-illuminated is designed

and fabricated. Through selective Zn diffusion to fabricate planar structure and precise charge layer design to adjust the internal electric field of the APD, the internal electric field of the device can be effectively confined inside the active region, which greatly suppresses the premature edge breakdown effect and reduces the dark current. By utilizing an absorption of 600 nm InGaAs and a multiplication of 100 nm InAlAs, the dark current at $0.9V_{\rm br}$ is reduced to 3 nA and the unit responsivity achieves 0.4 A/W. The maximum 3 dB bandwidth of 24 GHz and a GB product of 360 GHz are also achieved for this APD operating at 1.55 μm. It should be emphasized that the demonstrated device has an active area diameter of 15 μm. Such large active area diameter provides greater alignment tolerance for fiber coupling compared with using a waveguide structure.

Acknowledgements

This study was funded by the National Key R&D Program of China (Grant No. 2020YFB1805701) and the National Natural Foundation of China (Grant No. 61934003).

References

[1] Campbell J C 2016 *Journal of Lightwave Technology* **34** 278
[2] Waldrop J R, Kraut E A, Farley C W and Grant R W 1991 *J. Appl. Phys.* **69** 372
[3] Wang H, Yang X, Wang R, He T and Liu K 2020 *Opt. Express* **28** 16211
[4] Yagyu E, Ishimura E, Nakaji M, Ihara S, Mikami Y, Itamoto H, Aoyagi T, Yoshiara K and Tokuda Y 2009 *Journal of Lightwave Technology* **27** 1011
[5] Lahrichi M, Derouin E, Carpentier D, Lagay N, Decobert J, Glastre G and Achouche M 2009 35*th European Conference on Optical Communication (ECOC),* 2009 Sep 20–24, Vienna, AUSTRIA, p. 1
[6] Levine B F, Sacks R N, Ko J, Jazwiecki M, Valdmanis J A, Gunther D and Meier J H 2006 *IEEE Photonics Technology Letters* **18** 1898
[7] Li B, Lv Q Q, Cui R, Yin W H, Yang X H and Han Q 2015 *IEEE Photonics Technology Letters* **27** 34
[8] Nada M, Muramoto Y, Yokoyama H, Ishibashi T and Kodama S 2012 *Electron. Lett.* **48** 397
[9] Rouvie A, Carpentier D, Lagay N, Decobert J, Pommereau F and Achouche M 2008 *IEEE Photonics Technology Letters* **20** 455
[10] Tan L J J, Ong D S G, Ng J S, Tan C H, Jones S K, Qian Y and David J P R 2010 *IEEE Journal of Quantum Electronics* **46** 1153
[11] Campbell J C and Host C 2006 *Conference on Optical Fiber Communications/National Fiber Optic Engineers Conference*, 2006 Mar 05–10, Anaheim, CA, p. 2485
[12] Nada M, Yamada Y and Matsuzaki H 2018 *IEEE Journal of Selected Topics in Quantum Electronics* **24** 1
[13] Campbell J C 2008 *Optical Fiber Telecommunications V1A,* December 31, 2008, San Francisco, CA, USA: Academic, p. 221
[14] Nada M, Muramoto Y, Yokoyama H, Shigekawa N, Ishibashi T and Kodama S 2012 *Jpn. J. Appl. Phys.* **51** 02BG03
[15] Chen Y H, Wun J M, Wu S L, Chao R L, Huang J J S, Jan Y H, Chen H S, Ni C J, Chang H S, Chou E and Shi J W 2018 *IEEE Journal of Selected Topics in Quantum Electronics* **24** 1
[16] Tosi A, Calandri N, Sanzaro M and Acerbi F 2014 *IEEE Journal of Selected Topics in Quantum Electronics* **20** 192
[17] Jiang X D, Itzler M, O'Donnell K, Entwistle M, Owens M, Slomkowski K and Rangwala S 2015 *IEEE Journal of Selected Topics in Quantum Electronics* **21** 5
[18] Wang S, Ye H, Geng L Y, Lu Z Q, Xiao F, Xiao F and Han Q 2022 *Journal of Electronic Materials* **51** 2692
[19] Nada M, Muramoto Y, Yokoyama H, Ishibashi T and Matsuzaki H 2014 *Journal of Lightwave Technology* **32** 1543
[20] Nada M, Yoshimatsu T, Nakajima F, Sano K and Matsuzaki H 2019 *Journal of Lightwave Technology* **37** 260
[21] Achouche M, Decobert J, Vaissiere N, Martin F, Fortin C, Paret J F, Lanteri D, Mekhazni K, Gariah H, Caillaud C and Blache F 2019 *Optical Fiber Communications Conference and Exhibition (OFC)*, 2019 Mar 03–07, San Diego, CA, pp. 1–3
[22] Lahrichi M, Glastre G, Derouin E, Carpentier D, Lagay N, Decobert J and Achouche M 2010 *IEEE Photonics Technology Letters* **22** 1373
[23] Liu Y, Forrest S R, Ban V S, Woodruff K M, Colosi J, Erikson G C, Lange M J and Olsen G H 1988 *Appl. Phys. Lett.* **53** 1311
[24] Maruyama T, Narusawa F, Kudo M, Tanaka M, Saito Y and Nomura A 2002 *Opt. Eng.* **41** 395